Numerical and experimental investigation of the fluid dynamics in a Teniente type copper converter ☆

A. Valencia [a,*], M. Rosales [b], R. Paredes [b], C. Leon [b], A. Moyano [c]

[a] *Department of Mechanical Engineering Universidad de Chile, casilla 2777, Santiago, Chile*
[b] *Instituto de Innovación en Minería y Metalurgia Avenida del Valle No. 738, Santiago, Chile*
[c] *CODELCO, División Codelco Norte Chuquicamata, Chile*

Abstract

We have numerically studied and experimentally visualized the fluid dynamics in a Teniente type copper converter. The three-dimensional simulation of the three-phase system was carried out using the volume of fluid (VOF) and the standard k–ε turbulence models implemented in a commercial solver. The numerical model includes the white metal and slag liquid phases and gas phase through air injection from 50 submerged tuyeres. Experimental observation was carried out in a 1:5 scaled water container, and mean amplitude and frequency of bath oscillation were measured. The numerical simulation has been able to predict the axial displacement of slag layer, the bath oscillation and the jet formation.

Keywords: Copper converter; Fluid dynamics; Splashing

1. Introduction

The gas injected through the submerged tuyere line in Teniente type copper converter produces into the bath of molten matte a three-phase highly turbulent flow. Due the high gas inlet velocity the gas–liquid interaction causes jet formation and bath oscillation. The air flow affects the chemical and physical processes occurring in the converter such as converting rate, oxygen efficiency, mixing, splashing, and accretion build-up. Despite the importance of the interaction of the air jet and the matte in a converter, few studies of the fluid dynamics of converting process have been reported in the literature.

Zhao and Irons [1] reported the transition from bubbling regime to jetting regime when gas is injected into liquid at high velocity through a submerged tuyere. They found that the critical injection velocity for instability depends on surface tension, tuyere diameter, and the gas-to-liquid density ratio, which can be summarized by $We = 10.5(\rho_g/\rho_l)^{-0.5}$, where We is the Weber number based on tuyere diameter, ρ_g and ρ_l are the gas and liquid density respectively. Murai and Matsumoto [2] studied numerically the three-dimensional structure of a bubble plume. The results reveal several particular structures, such as swaying and swirling structures of the bubble plume.

☆ Communicated by W.J. Minkowycz.

* Corresponding author.
E-mail address: alvalenc@ing.uchile.cl (A. Valencia).

Nomenclature

A	Amplitude, mm
d	Tuyere diameter, m
D	Converter diameter, m
e	Slag layer thickness, mm
F	Volume fraction of one fluid
Fr	Froude number based on tuyere diameter, $u_o/[g(\rho_l/\rho_g-1)d]^{0.5}$
H	Water depth, mm
k	Turbulent kinetic energy, m^2/s^2
l	Jet penetration, mm
L	Converter length, m
s	Tuyere submergence, mm
w	Frequency, Hz
We	Weber number based on tuyere diameter, $\rho_g u_o^2 d/\sigma$
u_o	Velocity of gas in tuyere, m/s

Greek symbols

α	Dimensionless frequency
ε	Turbulent dissipation rate, m^2/s^3
μ_t	Turbulent viscosity, kg/m s
ρ_l	Density liquid phase, kg/m^3
ρ_g	Density gas phase, kg/m^3
σ	Surface tension coefficient, N/m

Themelis et al. [3] derived an equation to describe the trajectory of a gas jet in a liquid. They reported theoretical and experimental results for air jets injected into water for different Froude numbers. Hoefele and Brimacombe [4] have experimentally studied the behavior of gas discharging into a liquid. Two regimes of flow, bubbling and steady jetting have been delineated as a function of the Froude number and the ratio of gas to liquid densities. They have correlated the forward penetration of the jets with the equation: $l/d=10.7Fr^{0.92}(\rho_g/\rho_l)^{0.35}$, where Fr is the Froude number based on tuyere diameter. They concluded that low pressure blowing has the disadvantage of poor penetration of air into the bath so that the jets rise close to the back wall and locally accelerate refractory wear.

Brimacombe et al. [5] made experimental investigations involving the injection of air from a horizontal tuyere into water in a converted-shaped vessel. The experiments were conducted varying pct. filling and tuyere submergence to determine the critical air flow rate, above which bath slopping prevailed. They have shown that the critical air flow rate can be correlated with the buoyancy power per unit mass of the bath. Liow and Gray [6] carried out an experimental work in a 1:10 scaled water model of a Pierce-Smith copper converter, to study the influence of bath depth and tuyeres submergence on the formation of oscillations states (slopping), they reported the natural frequencies of bath oscillation as a function of liquid level of the reactor.

Rosales et al. [7] have conducted numerical simulations to study the gravity waves produced on bath free surface in the Teniente converter. The results show a good correlation with the experimental data. Longitudinal waves were formed due to the reflection and transmission of waves generated in the tuyere line zone. In a previous work, Valencia et al. [8] studied the fluid dynamics in a slice water model of the Teniente type copper converter with one submerged tuyere. They study the influence of Froude number on bath dynamics in particular with regard to flow mixing in the bath, jet stability, and splashing. The flow is characterized with an unsteady jet, which moves into wall directions and in some instances collapse.

In this work, we study the fluid dynamics in a Teniente type copper converter. The numerical model includes white metal and slag liquid phases and gas phase through air injection from 50 submerged tuyeres.

Experimental observation of the phenomena was carried out in a 1:5 scaled water container, and mean frequencies and amplitudes of bath surface oscillation are determined in four characteristic points of bath surface.

2. Mathematical model and geometry

In the VOF formulation [9] of multiphase fluid dynamics the fluids are not interpenetrating. For each phase in the model, a variable is introduced: the volume fraction of the phase in the computational cell. In each control volume, the volume fractions of all phases sum to unity. The fields for all variables and properties are shared by the phases and represent volume-averaged values, as long as the volume fraction of each of the phases is known at each location. Thus the variables and properties in any given cell are either purely representative of one of the phases, or representative of a mixture of the phases, depending upon the volume fraction values.

The VOF model uses the mass and momentum conservation equations for incompressible fluids to describe the fluid dynamics of both gas and liquid phase, that is,

$$\vec{\nabla}\cdot\vec{u} = 0 \tag{1}$$

$$\frac{\partial \rho\vec{u}}{\partial t} + \vec{\nabla}\cdot\rho\ \vec{u}\cdot\vec{u} = -\vec{\nabla}p + \mu\nabla^2\vec{u} + \rho\vec{g} + \vec{F}_{\mathrm{SF}} \tag{2}$$

here the properties of a fluid are given by

$$\rho(\vec{x},t) = F(\vec{x},t)\rho_{\mathrm{l}} + [1 - F(\vec{x},t)]\cdot\rho_{\mathrm{g}} \tag{3}$$

$$\mu(\vec{x},t) = F(\vec{x},t)\mu_{\mathrm{l,eff}} + [1 - F(\vec{x},t)]\cdot\mu_{\mathrm{g,eff}}. \tag{4}$$

Here, F is the local volume fraction of one fluid in the point (x, t). Its value is one in the liquid phase and zero in the gas phase. A value between 1 and 0 indicates a density interface. The subscripts l and g indicate liquid and gas phases, respectively. The model solves the scalar advection equation for the quantity F; this equation states that F moves with the fluid,

$$\frac{\partial F}{\partial t} + \vec{u}\cdot\vec{\nabla}F = 0. \tag{5}$$

The continuum surface force model is used to model the force due to surface tension F_{SF} acting on the gas–liquid interface. A similar approach is used to account for forces acting on the liquid due to wall adhesion. This model replaces the surface force due to surface tension with a continuous force F_{SF} acting on all fluid elements in the interface transition region,

$$F_{\mathrm{SF}} = \frac{\rho\sigma\kappa(\vec{x},t)\,\vec{\nabla}F(\vec{x},t)}{1/2(\rho_{\mathrm{l}} + \rho_{\mathrm{g}})}. \tag{6}$$

Thus, the surface tension force localized in the interface region is converted into a volume force with the help of a Dirac delta function concentrated on the surface. The curvature κ is defined in terms of the divergence of the surface normal of the secondary phase,

$$\kappa = \vec{\nabla}\frac{\vec{n}}{|\vec{n}|}. \tag{7}$$

In this research the standard k–ε turbulence model, extended for the use in multiphase systems, has been used [10]. This is a two-equation model based on transport equations for the turbulence kinetic energy, k, and its dissipation rate ε.

The transport equation for k is derived from an exact equation, while the transport equation for ε is obtained using physical reasoning. The equations for turbulent kinetic energy, k, and its rate of dissipation, ε, are:

$$\frac{\partial}{\partial t}(\rho k) + \frac{\partial}{\partial x_i}(\rho k u_i) = \frac{\partial}{\partial x_j}\left[\left(\mu + \frac{\mu t}{\sigma_k}\right)\frac{\partial k}{\partial x_j}\right] + G_k - \rho\varepsilon \tag{8}$$

$$\frac{\partial}{\partial t}(\rho \varepsilon) + \frac{\partial}{\partial x_i}(\rho \varepsilon u_i) = \frac{\partial}{\partial x_j}\left[\left(\mu + \frac{\mu_t}{\sigma_\varepsilon}\right)\frac{\partial \varepsilon}{\partial x_j}\right] + C_{1\varepsilon}\frac{\varepsilon}{k}G_k - C_{2\varepsilon}\rho\frac{\varepsilon^2}{k}. \tag{9}$$

In these equations, G_k represents the generation of turbulence kinetic energy due to the mean velocity gradients, $C_{1\varepsilon}$, $C_{2\varepsilon}$, σ_k and σ_ε are model constants. These values have been determined from experiments with air and water for

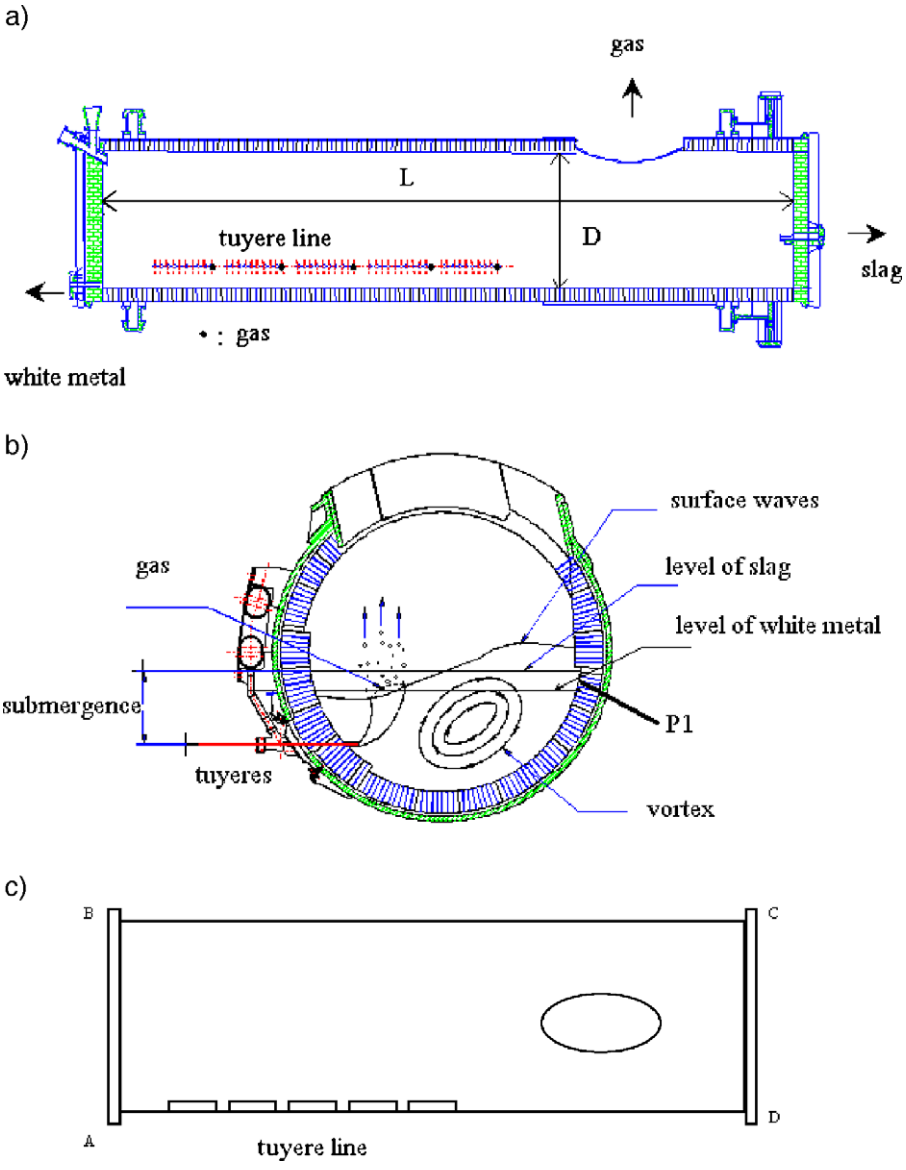

Fig. 1. Geometry of Teniente type copper converter.

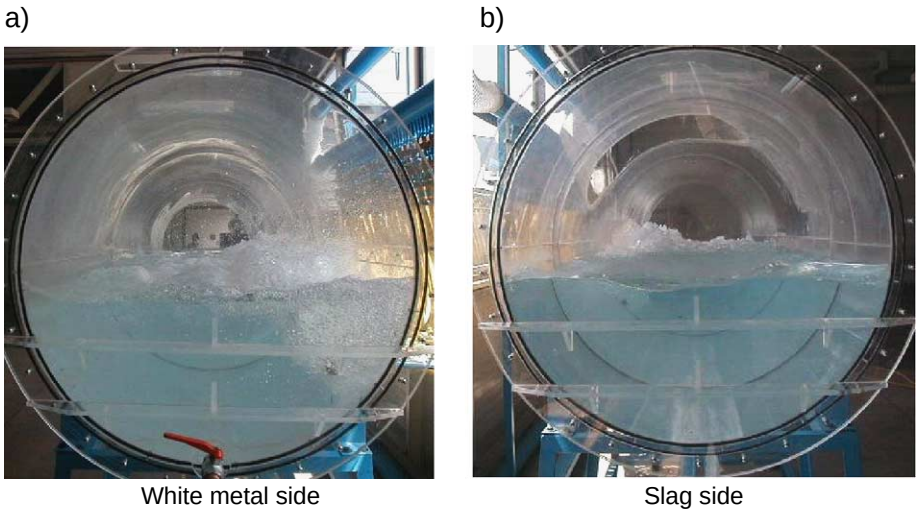

Fig. 2. Photographs in water model of bath oscillation, (a) white metal side, (b) slag side.

fundamental turbulent shear flows including homogeneous shear flows and decaying isotropic grid turbulence. In this model, the effective viscosity in the momentum equations is the sum of the molecular and turbulent viscosities

$$\mu_{\text{eff}} = \mu + \mu_{\text{t}} \tag{10}$$

with

$$\mu_{\text{t}} = \rho C_{\mu} \frac{k^2}{\varepsilon}. \tag{11}$$

Fig. 1 shows the Teniente type copper converter. It is a cylindrical vessel of $L=22$ m length with an inner diameter of $D=4.2$ m, the converter has an injection zone with 50 tuyeres and a settling zone. The submergence of the tuyere line is $s=990$ mm. In the actual operation condition the white metal level is 1250 mm, and the slag layer thickness is $e=450$ mm. We have considered $\rho=5200$ [kg/m^3] and $\mu=0.004$ [kg/m s] for the white metal, and $\rho=3000$ [kg/m^3] and $\mu=0.004$ [kg/m s] for the slag. The Froude number based on tuyere diameter is $Fr=8.6$. An experimental model scaled 1:5 was constructed and filled with water to perform fluid dynamics visualization.

3. Experimental and numerical setup

The experimental model of the Teniente copper converter was made of acrylic, in order to visualize the flow dynamics. Pictures were recorded with a digital video camera for later analysis. The amplitude and frequency of bath oscillations in 4 characteristic points of the free surface were determined, see Fig 1c. The air flow in the 50 tuyeres is obtained from a central manifold. The high pressure air line is obtained using two high pressure centrifugal ventilators, with an air flow of 600 m^3/h. The water level was set to $H=340$ mm, and the Froude number based on tuyere diameter was set to 8.6.

The VOF and the k–ε turbulence models were solved using the commercial solver Fluent 6.0. This package is a finite volume solver, using body-fitted grids. The grids are non-staggered and all variables are evaluated at the cell

Table 1
Mean amplitude, frequency and jet penetration at four points for the Teniente converter

A (mm), point A	A (mm), point B	A (mm), point C	A (mm), point D	w (Hz), point A	w (Hz), point B	w (Hz), point C	w (Hz), point D	l (mm)
550	454	376	449	0.58	0.54	0.49	0.45	280

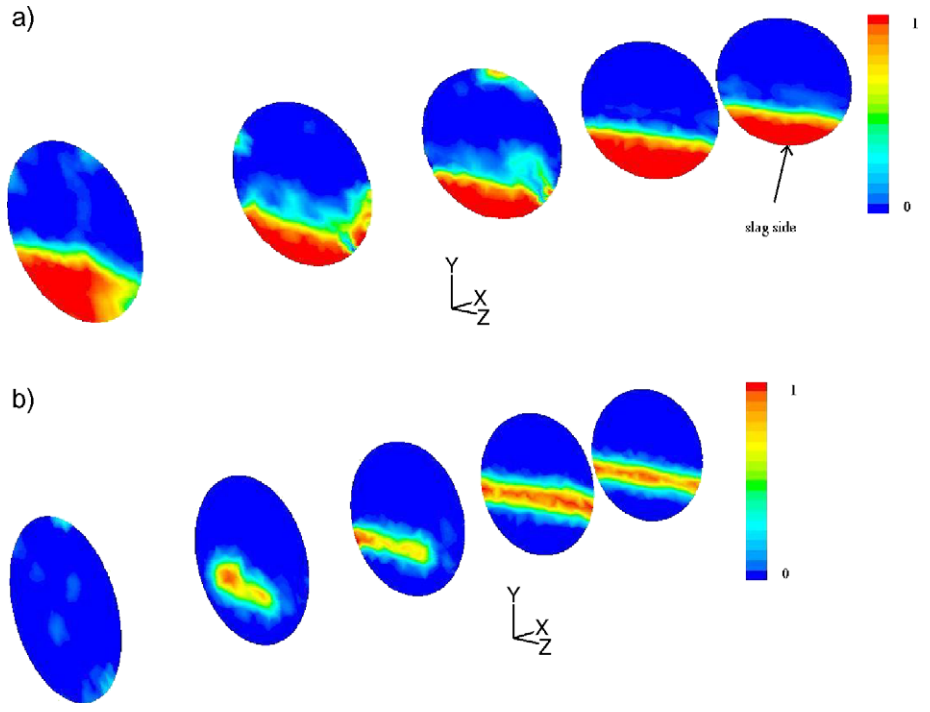

Fig. 3. (a) Contours of volume fraction of white metal, (b) contours of volume fraction of slag, for five different axial positions, t=21 s.

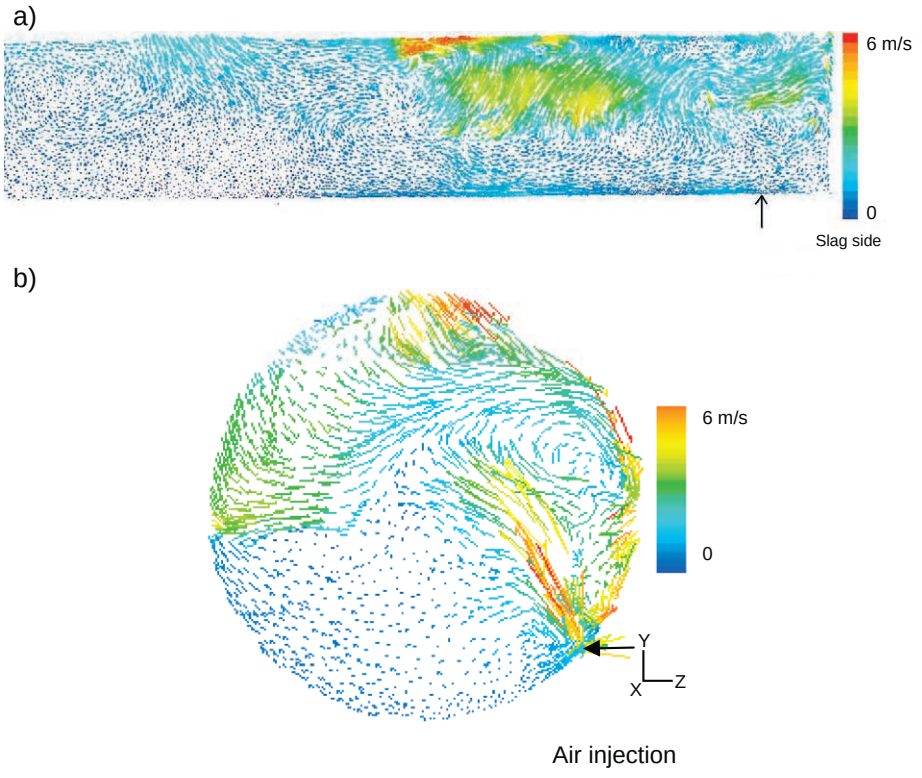

Fig. 4. (a) Velocity vectors colored by velocity magnitude at symmetry line, (b) velocity vectors at converter middle plane, X=11 m, t=21 s.

faces. The pressure–velocity coupling is obtained using the SIMPLEC algorithm. We use the geometrical reconstruction scheme to obtain the face fluxes, when the cell is near the interface between two phases; this scheme represents the interface between fluids using a piecewise-linear approach [10]. For the time dependent VOF calculations, we use the explicit time-marching scheme with two iterations per time step and with $\Delta t = 2 \times 10^{-4}$. The time step was computed from the Courant-Levy condition [11] from Eq. (12). With this small time step the residuals of

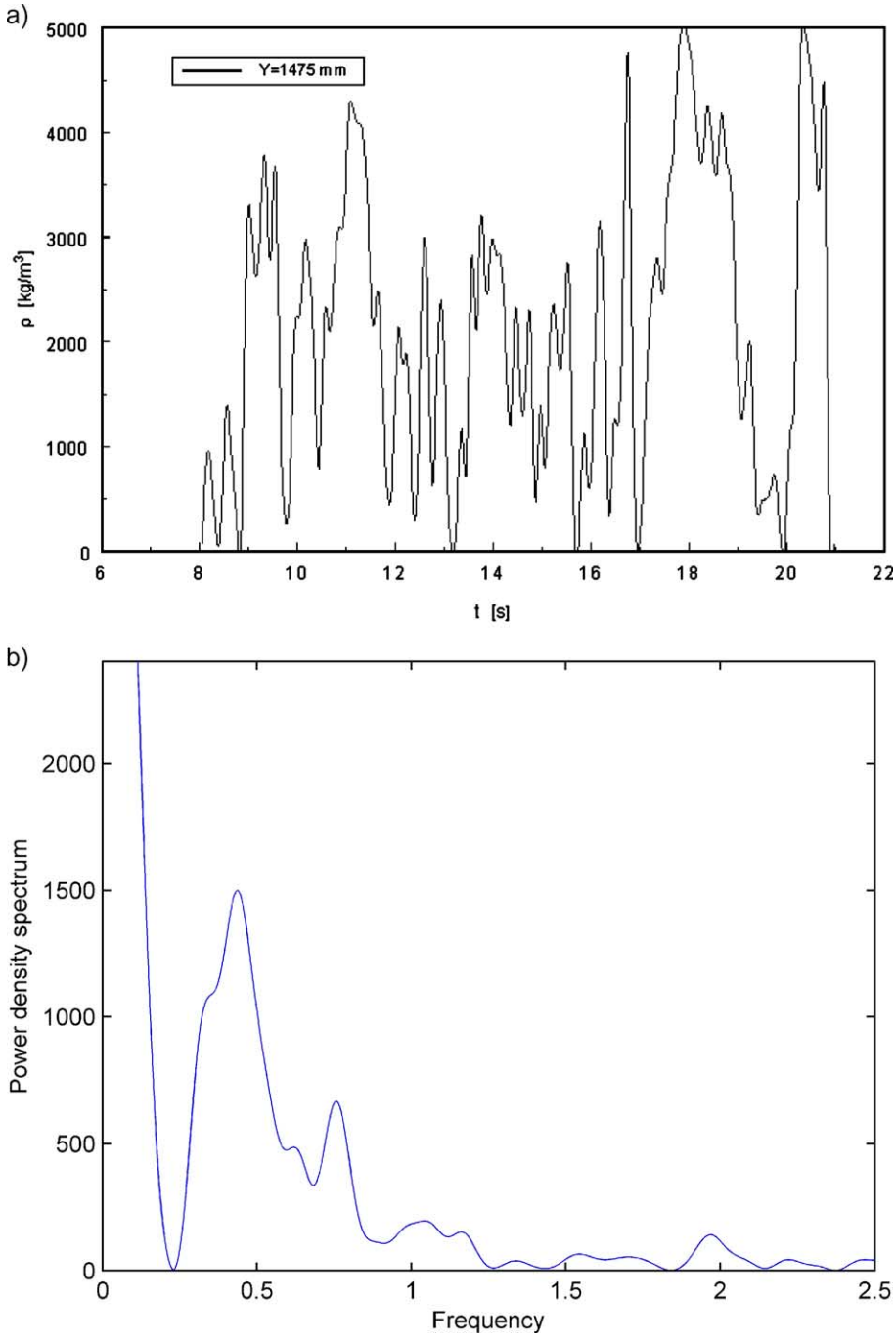

Fig. 5. (a) Variation of density with the time at converter middle plane in the point P1 (X=11 m, Y=1.475 m, Z=− 2.1 m) indicated in Fig. 1b, (b) power density spectrum of density in point P1.

the continuity and Navier-Stokes equations were smaller than 10^{-2} in all temporal iterations. We have used a grid of 112,987 control volumes; the mesh is composed of tetrahedral mesh elements. The computation of 21 s of operation of the converter model uses 2×10^5 iterations, and each iteration takes 8 s of CPU in a computer with Pentium IV processor and with Linux Red Hat 7.3 operating system.

$$\Delta t = \frac{\Delta x^2}{2(\mu/\rho) + U\Delta x}. \tag{12}$$

4. Results and discussion

Fig. 2 shows views from the white metal and the slag sides respectively of fluid dynamics in the water model. The air injection at white metal side produces turbulent jets, splashing and high air–water mix. The splashing and the gravity waves are dumping at the slag side of the converter. The mean values of amplitude of water oscillation, frequency and jet penetration were determined in the 4 points indicated in Fig. 1c. Using dimensional analysis [7], a dimensionless frequency can be defined as,

$$\alpha = \omega\sqrt{D/2g}. \tag{13}$$

Using Eq. (13) the experimental values of frequency can be transformed to representative values of frequency w for the Teniente type copper converter, the amplitude A and jet penetration l are obtained using the scale factor 5. Table 1 shows these mean values for the Teniente converter.

Fig. 3 shows instantaneous contours of volume fraction of white metal, Fig. 3a, and slag layer, Fig 3b, in five axial positions respectively for the time t=21 s. The numerical simulation can reproduce many characteristics of this unsteady three-dimensional and three-phase flow as: (i) air turbulent jets, (ii) splashing of free surface in the injection zone, (iii) suppression of splashing in the settling zone, (iv) displacement after t=21 s of the slag layer to the settling zone. The last finding is very important to be determined, so that the Teniente type copper converter can operate with this Froude number and with this level of white metal in an efficient way.

Instantaneous velocity vectors at two mean planes is shown in Fig. 4. The velocity vectors in the mean plane X–Y (Z=0) shows the complex vortex structure, in the gas phase it can be observed that the gas moves to the converter mouth. Maximal axial velocities of air, 6 m/s, are located near the roof of the converter. The velocity vectors in the mean plane Y–Z (X=11 m) show the air jet emerging in the white metal liquid phase, and the vortex structure formed in the gas phase. In the liquid phases the velocities are lower and vortex structures cannot be observed.

The variation of density in one point adjacent to the wall of the converter located in the mean plane Y–Z (X=11 m) in the position indicated in Fig. 1b is shown in Fig. 5a. The variation of density indicates that in this point the three phases are present in different instants. From the fast Fourier transform of this signal we obtain the dominant frequency of the density variation, see Fig. 5b, w=0.44 Hz. This numerical obtained frequency match very well the experimental values presented in Table 1. The differences are lower than 25% depending of the comparison point. Gravity waves were observed that travel in the axial direction of the converter from the white metal side to the slag side, in addition to the waves observed in the plane Y–Z of the converter.

5. Conclusions

We have conducted numerical simulations and experimental visualization to study the fluid dynamics in a Teniente type copper converter. We have studied the bath dynamics produced by air injection through 50 submerged tuyeres. The simulation was carried out using the volume of fluid and the standard k–ε turbulence model implemented in a commercial solver. The numerical simulation has been able to predict the axial displacement of slag layer, the bath oscillation and the jet formation.

Acknowledgments

The authors would like to thank the technicians of the Laboratory of fluid dynamics of IM2 for the assistance with the experimental work.

References

[1] Y. Zhao, G. Irons, The breakup of bubbles into jets during submerged gas injection, Metallurgical Transactions. B, Process Metallurgy 21B (1990) 997–1003.
[2] Y. Murai, Y. Matsumoto, Numerical study of the three-dimensional structure of bubble plume, Journal of Fluids Engineering 122 (2000) 754–760.
[3] N.J. Themelis, P. Tarassoff, J. Szekely, Gas–liquid momentum transfer in a copper converter, Transactions of the Metallurgical Society of AIME 245 (1969) 2425–2433.
[4] E. Hoefele, J. Brimacombe, Flow regimes in submerged gas injection, Metallurgical Transactions. B, Process Metallurgy 10B (1979) 631–648.
[5] J. Brimacombe, A. Bustos, D. Jorgensen, G. Richards, Toward a basic understanding of injection phenomena in the copper converter, Physical Chemistry of Extractive Metallurgy, TMS-AIME, Warrendale, PA, 1985, pp. 327–351.
[6] J. Liow, N. Gray, Slopping resulting from gas injection in a Pierce-Smith converter: water modeling, Metallurgical Transactions. B, Process Metallurgy 21B (1990) 987–996.
[7] M. Rosales, P. Ruz, R. Fuentes, A. Valencia, A. Moyano, J. Bobadilla, Gravity waves in the Teniente converter, Pyrometallurgy of Copper, Book, vol. 2, COPPER 2003, Santiago, Chile, 2003, pp. 485–498.
[8] A. Valencia, R. Paredes, M. Rosales, E. Godoy, J. Ortega, Fluid dynamics of submerged gas injection into liquid in a model of copper converter, International Communications in Heat and Mass Transfer 31 (2004) 21–30.
[9] E. Delnoij, J. Kuipers, W. Swaaij, Computational fluid dynamics applied to gas–liquid contractors, Chemical Engineering Science 52 (1997) 3623–3638.
[10] Fluent 6.0 User's guide 2001, chapters 10, 22.
[11] J. Ferziger, M. Periç, Computational Methods for Fluid Dynamics, Springer, Verlag, 1997, pp. 135–140.